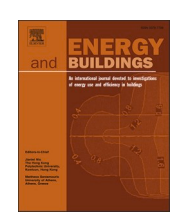
ELSEVIER

Contents lists available at ScienceDirect

# **Energy & Buildings**

journal homepage: www.elsevier.com/locate/enb





# Experimental performance of a new mixed-flow two-stage regenerative indirect evaporative cooler

Ana Tejero-González <sup>a,b,\*</sup>, Manuel Andrés-Chicote <sup>a</sup>, Eloy Velasco-Gómez <sup>a</sup>, Alessandra Urso <sup>a,b</sup>, Vincenzo Costanzo <sup>b</sup>, Gianpiero Evola <sup>c</sup>, Francesco Nocera <sup>b</sup>

- <sup>a</sup> Department of Energy Engineering and Fluidmechanics, Grupo de Investigación de Termotecnia, ITAP, Escuela de Ingenierías Industriales, Universidad de Valladolid 47011 Valladolid. Spain
- <sup>b</sup> Department of Civil Engineering and Architecture (DICAR), University of Catania 95125 Catania, Italy
- <sup>c</sup> Department of Electrical, Electronics and Computer Engineering, University of Catania 95125 Catania, Italy

#### ARTICLE INFO

#### Kevwords:

Dew Point Indirect Evaporative Cooler Multiple stage Experimental characterization Thermal effectiveness Cooling capacity

#### ABSTRACT

Evaporative cooling can improve energy efficiency in buildings; however, the air supplied to indoor spaces may be excessively humid or not cool enough to ensure thermal comfort. To overcome this, Indirect Evaporative Coolers maintain a constant humidity ratio at the product airstream, and regenerative airflow configurations allow cooling below the inlet air's wet bulb temperature. Such devices rely on the well-known Maisotsenko cycle and are often referred to as Dew Point Evaporative Coolers, as they can ideally reach the dew point temperature of inlet air. This work proposes a mixed-flow prototype that combines the superior thermal performance of counter-flow designs with the compact size of cross-flow systems. The heat exchanger is made of polycarbonate plates, while water distribution is optimized thanks to outlet nozzles and a wicking material placed on the wet side of such plates. The device has a volume of  $0.025~\text{m}^3$  and supplies 40~l/s of cooled air, achieving a cooling capacity greater than 325 W under inlet air conditions of 40 °C and 30 % relative humidity, with a water consumption of 1.9 l/h. Experimental results demonstrate that increasing the inlet dry bulb temperature and decreasing the inlet air relative humidity significantly improve temperature drop and cooling capacity, though they have a limited effect on the thermal effectiveness. Compared to a previous one-stage prototype, the twostage configuration increases the temperature drop and both the wet bulb and dew point effectiveness by about 50 %. However, the cooling capacity barely improves less than 17 %, due to the use of part of the product air as working air.

# 1. Introduction

To reduce energy consumption in buildings, increasing attention is paid to the use of energy efficient strategies for cooling and ventilating indoor spaces, such as evaporative cooling. However, despite their multiple advantages, evaporative cooling devices face several limitations, including non-negligible water use, maintenance needs, dependence on operating climate conditions, and challenges in complying with supply air requirements [1].

In this line, Indirect Evaporative Coolers (IEC) are on the spotlight because of their ability to cool the supply air only through sensible heat transfer, thereby avoiding humidification of the indoor space [2,3]. Moreover, they broaden the applicability of evaporative cooling to a

wider range of climate conditions when operating with the return air from the conditioned space as the secondary airstream. This operation mode is known as recovery IEC [4]. Yet, the lowest supply air temperature achievable in this mode is limited by the wet bulb temperature of the secondary airstream at the inlet.

This limitation in the supply air temperature can be overcome by using a fraction of the product air as working air on the wet side of the heat exchanger [5,6]. This airflow arrangement is called regenerative IEC [7]. When applied in multiple consecutive stages, the product air can ideally reach the dew point temperature of the primary air at the inlet. These systems are commonly called "Dew Point Indirect Evaporative Coolers", and rely on the well-known Maisotsenko cycle [5,6], which pioneered and continues to lead the market in this technology. By pre-cooling the working airstream with a fraction of the dry-channel air,

E-mail address: ana.tejero@uva.es (A. Tejero-González).

<sup>\*</sup> Corresponding author at: Department of Energy Engineering and Fluidmechanics, Grupo de Investigación de Termotecnia, ITAP, Escuela de Ingenierías Industriales, Universidad de Valladolid, 47011 Valladolid, Spain.

Nome	nclature	aw	working air
		d	dry channel
Α	Heat Exchange area (m²)	da	dry air
CC	Cooling Capacity (W)	dp	dew point
H	Height (cm)	HX	heat exchanger
L	Length (cm)	in	inlet
ṁ	Air mass flow rate (kg/s)	out	outlet
p	Pressure (Pa)	SET	setpoint
P	Electric power (kW)	v	vapor
RH	Relative humidity (%)	W	wet channel
T	Temperature (°C)	wb	wet bulb
$\dot{V}$ $v$ $w$ $W$ $\delta$ $\Delta p$ $\epsilon$	Air volume flow rate (m³/s) Specific volume (m³/kg) Humidity ratio (g/kg) Width (mm) Plate thickness (mm) Pressure drop (Pa) Thermal effectiveness (-)	Acronym DBT DPIEC IEC OP RSS TH	Dew Point Temperature Dew Point Indirect Evaporative Cooler Indirect Evaporative Cooler Orifice Plate Root Sum Square Temperature and Humidity sensor
Subscri	pts	TFL	Technology Readiness Level
ар	product air	WBT	Wet Bulb Temperature

the Maisotsenko IEC design enables the supply air temperature to drop below the wet bulb temperature limit, besides avoiding additional moisture. Moreover, pressure drop can be reduced by perforating the working channels. Although this concept can be implemented either in a counter-flow or cross-flow configurations, counter-flow designs present certain challenges in design and manufacturing. As a result, cross-flow Maisotsenko cycle air coolers were the first to be commercialized [8].

# 1.1. Design issues: Airflow configuration, length, water distribution, and wicking

Addressing the limitations of evaporative cooling phenomenon often leads to complex designs, which undermines one of the major advantages of the most elementary applications: their simplicity. The key aspects to be addressed in the design of regenerative IEC systems include airflow configuration(generally counter-flow or cross-flow), geometry, material selection, and water distribution to and through the wet channels, which can be enhanced by the use of wicking materials [,9].

The airflow configuration can be either counter-flow or cross-flow. In the counter-flow configuration, the two airstreams flow in opposite directions, while in the cross-flow configuration the secondary airflow runs perpendicular to the primary airflow [3]. For regenerative (or dew point) systems, the counter-flow configuration generally achieves better performance. However, cross-flow is recognized as less bulky, with lower friction losses and a simpler design, making it the first available option in the market [5]. Some studies have also explored alternative configurations. For instance, Jia et al. [10] developed a counter-cross-flow prototype that achieved better performance than cross-flow and comparable results to counter-flow, while reducing size and weight for the same air flow rate. Similarly, Deepak et al. [11] proposed a mixed-flow configuration that showed effectiveness comparable to previous research on cross-flow and counter-flow configurations.

Some published research have analysed performance improvements associated with increasing channel length. Most of these results were obtained through simulations performed for different lengths, using models previously validated with experimental data for a given reference length. Overall, findings indicate that increasing length has a positive effect on the performance of both cross-flow [12] and counterflow [13,14] configurations. However, for counter-flow, Zhan et al [15] observed that the effect of increased length appeared negligible beyond 1 m. Jafarian et al. [16] simulated channel lengths from 400 to 600 mm

and observed that shorter devices reduced contact time and consequently temperature drop, but underlined the also lower friction loss. Moreover, Zhu et al. [17], through experiments on counter-flow test-rigs of different lengths, found that a 400 mm device was preferable, as it was as it was sufficient to nearly saturate the working airstream. Gao et al. [18] evaluated the effect of increasing the channel length up to 1000 mm in counter-flow tube- and plate-type dew point evaporative coolers, and identified that for plate-type heat exchangers the working air reached saturation after about 300 mm, while in tube-type systems saturation occurred much earlier, after only 50 mm.

Water distribution is another key aspect of the design. The wet channels must be completely wetted to ensure maximum contact between air and water; however, excessive water flow can form thick water films that increase thermal resistance and may even block the channels [19]. Under these undesirable conditions, the water inlet temperature would be decisive, because the evaporation rate decreases and heat transfer becomes predominantly sensible [20,21]. Consequently, both the water flow rate and its distribution should be optimized to ensure uniform humidification while avoiding excessive water

To this aim, different water distribution strategies and the use of wicking materials are proposed in the literature [5,6]. According to existing results, higher evaporation should be expected when water is supplied transversely to the airflow [22] with continuous supply. However, intermittent spraying can reduce the energy consumption [23], and resulted preferable in porous ceramic IEC, as observed by Sun et al. [24]. Careful selection of nozzles is also essential. In the same experimental work from Sun et al. [24], a spiral-type nozzle was the optimal choice, whereas Ma et al. [25] identified the optimum nozzle parameters of 0.25 mm droplet diameter, 1.5 bar pressure, 5.4 l/min flow rate, and 68° cone angle through a 3D Computational Fluid Dynamics model. Moreover, 80 mm spacing between nozzles was proposed. Alternatively, Xu et al. [26] integrated the water distributor directly within the wet channels, using thin tubes with small openings. Beyond the selection and arrangement of the nozzles, the use of wicking materials over the wet channels surface has been targeted as a useful way to uniformly distribute the water through capillarity [6]. With this aim, fibres have been shown to balance the water absorption, diffusion ability, and mechanical strength [5]. For the polycarbonate plates used in the present work, previous research [27] showed that the performance improved with the use of nozzles outside the wet channels,

together with a cloth fabric placed on the wet side of the heat exchanger. Due to its low cost and wide availability, cotton cloth was selected as the wicking material.

# 1.2. Improving the performance through multiple stages/ middle perforations

One of the advantages of counter-flow and mixed-flow configurations is that intermediate bleedings of the primary air can be implemented by perforating orifices at different distances from the inlet section, yielding a multiple stages regenerative IEC.

Although the use of multiple stages can enhance the dew point performance of regenerative IEC, the available literature analysing this effect is scarce, and most studies correspond to simulations based on mathematical models validated with experimental results from one-stage devices. Zhou et al. [28,29] evaluated the effect of placing perforations in the middle section of a counter-flow regenerative IEC, thereby creating a two-stage system. Simulations were performed on a model validated with experimental data from a one-stage,800 mm long device. They showed that when a hole was placed at the middle section, the product air temperature was further decreased by 2.3 °C.

When more than two-stages are considered, results reported in the literature sometimes diverge. For instance, Cui et al. [30,31] simulated the effect of multiple stages in both conventional and regenerative (or dew point) IEC, considering different channel lengths. They validated their model with experimental results on a 750 mm long one-stage device. Simulations showed that multiple stages improved thermal effectiveness, increased pressure drop and reduced cooling capacity. Based on their findings, a maximum of three stages would be recommendable for conventional IEC arrangements, while for regenerative IEC, a maximum of two stages would be preferable. However, Oh et al. [32] focused on two alternative four-stage (or "purge") arrangements compared to a single stage, and their simulations showed that the temperature drop increased as the purge ratio (or working-to-inlet air ratio) increased.

The literature approaching multi-stage regenerative IEC is summarised in Table 1.

The position of the perforations can be crucial in multiple-stage DPIEC. In this sense, special attention should be paid to the work of Dizaji et al. [21] because their simulations were performed on a model validated with experimental results from a two-stage test rig. The device was 1000 mm long and the first-stage orifices were located 500 mm

 Table 1

 Published literature on multiple-stage regenerative IEC.

Work	Number of stages	Type of work	Results
Dizaji et al. [21]	2	Experimental and simulation	Perforations at the end of the dry channel yields better temperature drops than perforations placed in the middle.
Dizaji et al. [20]	1, 3	Simulation	The location of perforations (multi-stage) is crucial for the temperature drop and differs between laminar and turbulent airflows.
Cui et al. [30,31]	1	Experimental	Multi-stage arrangement improves thermal effectiveness
	2	Simulation	without decreasing the cooling capacity. Optimal number of stages for regenerative IEC is two.
Zhou et al. [28,29]	1	Experimental	Simulation results of placing middle perforations increases the
	2	Simulation	water evaporation, improving the cooling effect.
Oh et al. [32]	1	Experimental	Increasing the purge (working-to- inlet air ratio) decreases the
	4	Simulation	product air temperature.

from the air inlet. They observed that moving the middle perforations closer to the end of the dry channel enhanced the temperature drop in the primary air.

There is additional research examining the effect of perforation position; however, it does not focus on multiple-stages. For instance, the results of Liu et al. [33] showed that placing the orifices farther from the air inlet had a positive effect on thermal performance, although negatively influenced system friction. Nevertheless, the optimal location of the perforations would differ between laminar and turbulent flows [20]. Finally, Anisimov et al. [34] evaluated alternative configurations of the Maisotsenko cycle, including regenerative heat exchangers with and without perforations. They obtained slightly higher product air temperatures when perforations were placed along the heat exchanger, although the same overall length was used in both cases.

# 1.3. Novelty and scope of the article

As discussed in the previous section, a regenerative airflow arrangement can expand the potential of an Indirect Evaporative Cooler. However, it entrains additional complexity into system design. The literature reveals that multiple-stage arrangements can further improve the performance of regenerative IECs, yet most available results come from simulations based on models validated with one-stage test-rigs.

The present work aims at filling this gap by providing experimental evidence on the performance of a two-stage regenerative IEC made of polycarbonate plates. A new mixed-flow arrangement was selected to combine the compact size and simpler design of a cross-flow device with strong thermal performance. To ensure uniform water distribution, the system uses outlet nozzles and cotton wicking material.

The Methodology section exhaustively describes the system's design and dimensions, as well as the testing procedures, to enable future researchers or users to reproduce both the device and the study. All measured results are shared as open data. The Results and discussion section presents the performance of the prototype, compares it to that of a previous one-stage mixed-flow device with the same water distributor and materials, and contrasts it with experimental evidence on two-stage arrangements available in the literature.

The scope of this work is focused on the thermal characterization of a novel two-stage regenerative IEC laboratory prototype. As a secondary objective, comparison to previous relevant designs is presented. In this regard, the study aims to evaluate the potential to expand the range of inlet air conditions under which adequate supply air conditions can be achieved, based on the increased cooling capacity of the two-stage prototype compared to one-stage devices. Moreover, as low-TRL (Technology Readiness Level) research, the proposed system is not yet ready for commercialization, and a detailed evaluation of its environmental or economic aspects has not been carried out, as these are beyond the scope of this work.

# 2. Methodology

# 2.1. Description of the prototype

A new design of a two-stage regenerative IEC with mixed-flow configuration has been conceptualized and a prototype has been built with polycarbonate plates. Based on the results from previous prototypes [27], the wet channels are covered with a wicking material, namely cotton cloth, and outlet nozzles are chosen for the water distribution system. The design characteristics are summarized in Table 2.

As outlined in the Introduction, the regenerative configuration of an Indirect Evaporative Cooler (IEC) consists of diverting a portion of the inlet (primary) air at specific points in the dry air channels to the wet channels to create the secondary (or working) air stream. As a result, the inlet air stream splits into: (i) the main product air, sensibly cooled in dry channels by heat transfer to the secondary flow, and (ii) the secondary working air, drawn from the primary stream, exchanging heat

**Table 2**Description of the design characteristics of the Indirect Evaporative Cooling prototype.

Air flow configuration	Mixed-flow regenerative
Number of stages	2
Design working-to-inlet air ratio	0.6
Material of the heat exchanger	Polycarbonate
Wicking material on wet channels surface	Cotton cloth
Water distributor type	Water spraying over the wet channels' outlet (7 six-stream nozzles)

and moisture in wet channels, and then exhausted. In a two-stage device, the primary airstream is bled and diverted as working air twice before exhausting the system as product air. In the present prototype, a minimum working-to-inlet air ratio of 0.6 is achievable by design. Higher values of this operating parameter, meaning a greater fraction of working air and a smaller fraction of product air, could be obtained by adding external pressure drop to the product air duct.

Fig. 1 shows different schematic views of the prototype, which consists of a Plate Heat Exchanger (PHX). Fig. 1.a. presents a global view of the geometry and dimensions of the proposed unit, indicating the inlet and outlet sections of the different air streams (inlet, working and product air). The inlet air enters the device through an inlet section of  $18~\rm cm \times 23~\rm cm$  and flows along 60 cm polycarbonate plates. As it moves forward, it splits into two streams: the working air, which exits through the upper section (23 cm  $\times$  60 cm), and the product air, which leaves the unit through the opposite end, downstream of the inlet. Fig. 1.b. provides a detailed view of the dry and wet channels. The dry channels (in

orange) receive the inlet air and are arranged vertically between alternating plates, extending to the product air outlet. These channels are delimited by additional thin polycarbonate walls that improve air stream guiding in the primary flow direction. The wet channels (in green) occupy the remaining gaps between plates and are not delimited by additional walls, so the working air stream flows freely along the open space between plates and exits through the upper end of the unit. Finally, Fig. 1.c. shows a schematic detail of how the working air flow is bled from the primary air stream and driven into the wet channels. It can be observed that several dry channels are perforated at a middle and end positions along the primary air path, enabling a portion of the primary air to enter the wet channels and act as working (secondary) air. Owing to the location of the working air outlet, the secondary flow moves from the plate orifices toward the upper end of the unit, following an air path that is characteristic of a mixed-flow configuration, meaning that it is considered and mix between pure counter-flow and pure cross-flow arrangements. It should be noted that the wet channels are kept moist by an upper water distribution system.

Fig. 2 shows photographs of the actual prototype including the detail of one of the polycarbonate plates with the diverting orifices in the dry channels (Fig. 2.a), as well as a global view of the assembled prototype (Fig. 2.b).

The geometric dimensions included in Fig. 1 and other design values are provided in Table 3.

# 2.2. Experimental setup and performed tests

Once assembled, the prototype is mounted on a structure made of PVC and connected with flexible ducts to an Air Handling Unit (AHU)

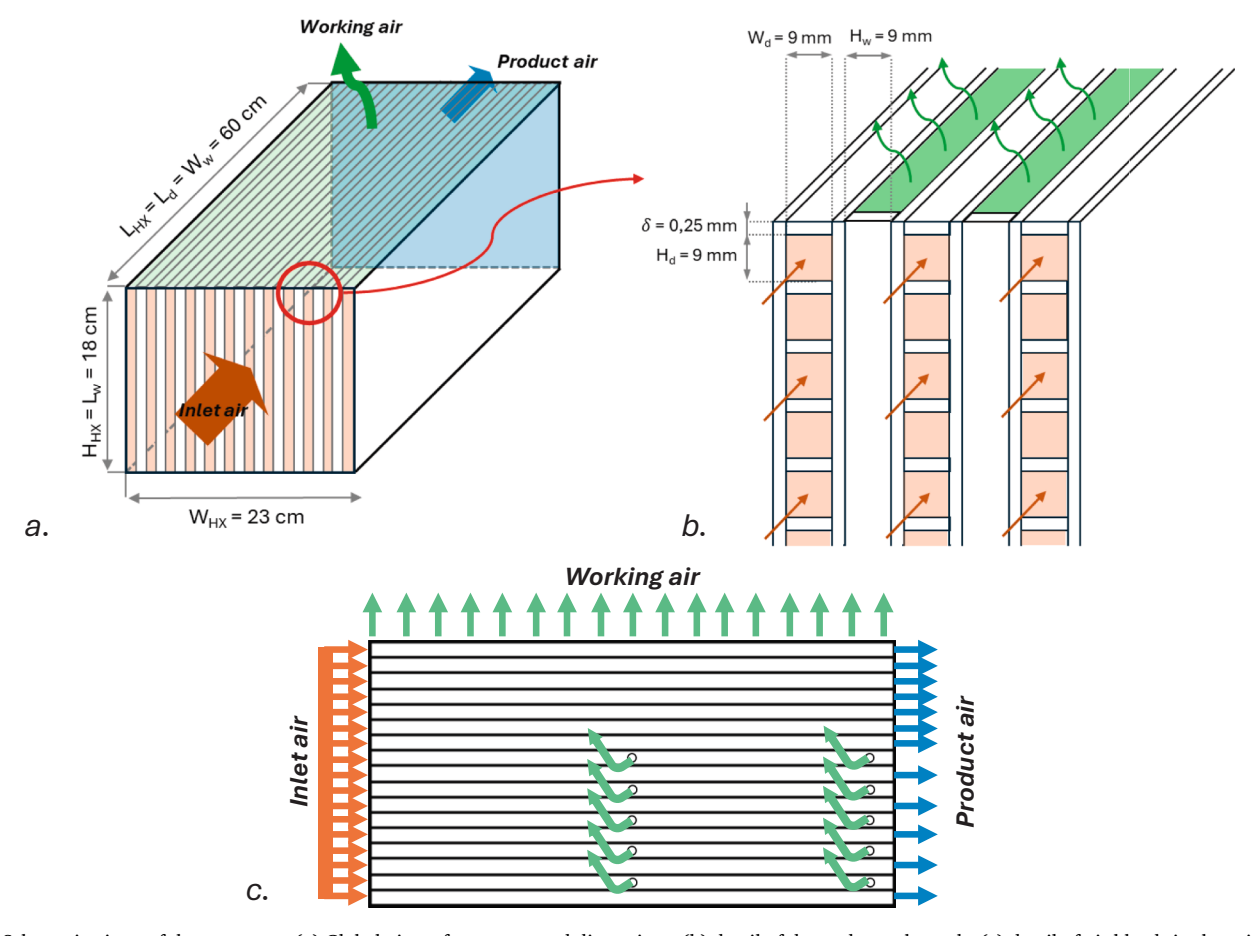


Fig. 1. Schematic views of the prototype: (a) Global view of geometry and dimensions, (b) detail of dry and wet channels, (c) detail of air bleeds in the primary air stream at middle and end positions of the dry channels.





**Fig. 2.** Actual DPIEC prototype: (a) Detail of one polycarbonate perforated plate and (b) global view of the assembled prototype including the water distribution system.

**Table 3**Geometric dimensions of the prototype.

Parameter	Value	Units
Total dimensions of the assembled heat exchanger (L <sub>HX</sub> x W <sub>HX</sub> x H <sub>HX</sub> )	60 x 23 x 18	cm <sup>3</sup>
Number of dry plate gaps	12 gaps	
Number of dry channels	18 (channels/gap) ×	_
•	12 gaps	
Dry channel length* (L <sub>d</sub> )	60	cm
Dry channel width* (W <sub>d</sub> )	0.9	cm
Dry channel heigth (H <sub>d</sub> )	0.9	cm
Number of wet channels	11	_
Wet channel length* (Lw)	18	cm
Wet channel width* (Ww)	60	cm
Wet channel heigth (H <sub>w</sub> )	0.9	cm
Plate wall thickness ( $\delta$ )	0.25	mm
Number of first stage perforations per dry channel	5	_
Position of first stage perforations (distance from air inlet)	25	cm
Diameter of first stage perforations	5	mm
Number of second stage perforations per dry channel	5	_
Position of second stage perforations (distance from air inlet)	56	cm
Diameter of second stage perforations	5	mm

 $<sup>^*</sup>$ Channel length and width dimensions should be understood for each airstream as: Length (L) = dimension along the airflow direction; Width (W) = dimension across the airflow direction.

that reproduces the inlet air conditions to be tested. The water distribution system is fed with a 24 W and 12 V DC water pump from a lower tank that collects the remaining water that does not evaporate inside the wet channels. A scheme of the whole experimental setup can be seen in Fig. 3.

Calibrated orifice plates are installed at the inlet  $(OP_{in})$  and outlet  $(OP_{out})$  air ducts to determine the total (inlet) and the product (supply) air volume flow rates, by measuring the pressure drop across each orifice plate. They were calibrated using a reference nozzle by correlating the flow rate measured in the nozzle with the pressure drop across the orifice plates, thus determining the constant that relates the airflow rate to the square root of the pressure drop in the orifice plate:

$$\dot{V}_{ap} = k \bullet \sqrt{\Delta p_{ap}} \tag{1}$$

Where k is the characteristic of the calibrated orifice plate.

The total and product air mass flow rates are then obtained by dividing the corresponding volumetric air flow rates by the specific volume calculated under the inlet and product air psychrometric conditions, respectively:

$$\dot{m}_{qp} = \frac{\dot{V}_{qp}}{V_{qm}} \tag{2}$$

Dry bulb temperature and relative humidity sensors are placed at the inlet section (TH $_{\rm in}$ ), at the outlet of the product air flow (TH $_{\rm out}$ ), and at the outlet of the working airflow (TH $_{\rm out}$ (2), TH $_{\rm out}$ (3)). All temperature and humidity probes were also conveniently calibrated. Temperature calibration was performed using a FLUKE 9103 dry-well calibrator (calibration range:  $-25~^{\circ}\text{C}$  to 140  $^{\circ}\text{C}$ ), while relative humidity probes were calibrated by exposing the sensors to thermodynamically stable environments generated with saturated salt solutions (LiCl, MgCl $_2$  and  $K_2SO_4$ ).

The specifications of the measuring equipment are provided in Table 4.

A total of 23 tests were performed with different inlet dry bulb air temperature and relative humidity values. The inlet air flow rate supplied by the AHU is kept at  $5.9\pm0.2~m^3/\text{min}$ . For the present two-stage mixed-flow design, the working-to-inlet air ratio (R) was consistently measured and resulted to vary within  $0.61\pm0.03$  among the tests. This yields a product airflow of approximately  $2.4~m^3/\text{min}$  (40 1/s).

Because the working-to-inlet air ratio is defined as the ratio between the working  $(m_{aw})$  and the total inlet  $(m_{in})$  air mass flow rates, it is calculated from the measured product air and inlet air flow rates (Equation (3):

$$R = \frac{\dot{m}_{av}}{\dot{m}_{in}} = 1 - \frac{\dot{m}_{ap}}{\dot{m}_{in}} \tag{3}$$

Tests were conducted in Valladolid, Spain (690 m.a.s.l.). To broaden the applicability of the results beyond the climate conditions of the location (Csa: Temperate, dry and hot summers), inlet air dry bulb temperature and relative humidity are varied within a wider range. Table 5 presents the setpoints and measured air temperature and humidity conditions used in the tests. Five tests are conducted at each inlet air DBT level with varying inlet air humidities. For a DBT of 35 °C, however, eight tests are performed to evaluate the effect of inlet RH over a broader range.

The AHU's electric heater, regulated by a PID controller, ensures that the desired inlet air DBT setpoint is achieved with high precision and minimal variation. The control probe used for the AHU's supply temperature was placed at the inlet of the evaporative cooler, thus minimizing the impact of heat losses between the AHU outlet and the inlet of the tested prototype. In addition, the inlet air RH is controlled using a vapour injection humidifier, with its electrical power input adjusted for each humidity level.

The tested range of inlet DBT and RH shown in Table 5 is intended to reproduce a broad sweep of conditions representative of various summer climates where air cooling is required to achieve thermal comfort. Regarding the physiological evaluation of the climate [35], mild, warm, hot, sultry and extremely hot climates would be covered.

# 2.3. Description of the testing procedure

The procedure followed during each experimental test is described below.

 The start time for data logging in the TH sensors was set, with measurement intervals of 10 s. The data recording start time was always set before the beginning of the tests to verify that the probe

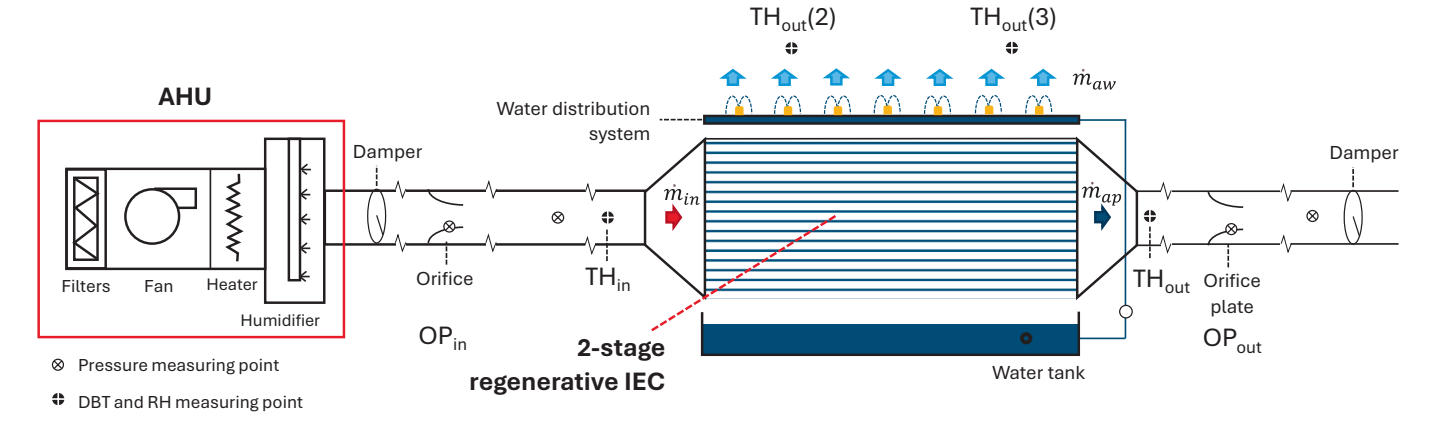


Fig. 3. Scheme of the experimental setup.

**Table 4**Characteristics of measuring equipment.

Parameter	Measuring equipment	Range	Accuracy
Air dry bulb temperature	Testo 175 H1 Temperature and relative humidity sensor	−20–+55 °C	±0.4 °C
Air relative humidity	Testo 175 H1 Temperature and relative humidity sensor	0 %–100 %	$\pm 2\%$ RH (from 2 %– 98 % RH) at $+$ 25 $^{\circ}\text{C}$
Water temperature	Testo 175 T2 Temperature sensor	−35–+55 °C	±0.5 °C
Static pressure	Data logger Testo 435–4	0–25 hPa	±0.02 hPa (0–2 hPa) ±1% of measured values (remaining range)

**Table 5**Tests inlet air conditions.

Inlet DBT setpoint (T <sub>in,SET</sub> )	Measured inlet DBT (T <sub>in</sub> )	Vapor injection electric power setpoint (P <sub>v,SET</sub> )	Measured inlet RH (RH <sub>in</sub> )	Number of tests performed	Inlet humidity ratio (w <sub>in</sub> )
[°C]	[°C]	[kW]	[%]	[-]	[g <sub>v</sub> /kg <sub>da</sub> ]
25	24.8-25.1	0	41-52	5	8.7–11
30	29.6-29.9	0, 1.5	35-59	5	9.8-16.9
35	34.4-34.9	0, 1.5, 2,	32-72	9	11.8-27.3
		3, 4.5, 6			
40	39.2–39.5	0, 2, 4	23–40	5	11–19.7

readings were consistent with the ambient conditions at their locations.

- 2) The AHU was started, and the specific inlet air flow rate and inlet air DBT (that is, the specific conditions of the air flow entering the prototype) were set. Within this process, the following actions were carefully applied:
  - 2.1) The fan was switched on.
  - 2.2) The temperature controller was switched on, and the setpoint for the inlet air DBT supplied to the evaporative cooler was configured.
  - 2.3) Tests always began without humidity control (humidifier off). For tests requiring humidity control, the humidifier was switched on and adjusted to the desired humidification power.
  - 2.4) The dampers were adjusted to achieve the target total and product air flow rates for the test by measuring the pressure

drop across the two orifice plates at the prototype's inlet and outlet.

The test duration was sufficient to ensure that steady-state temperature and humidity conditions were reached in the air streams under the established operating conditions. Pressure drop was repeatedly measured throughout the test to verify that airflow rates remained constant.

Once the test was completed, the AHU was switched off, and the data stored in the TH data loggers were downloaded.

For the calculations, the temperature and relative humidity values correspond to the mean values recorded over a 20-minute steady-state period (120 measurements). As an illustrative case, Fig. 4 and Fig. 5 depict the temporal evolution of temperature and humidity, respectively, during a representative test conducted on October 25th, 2024, from the onset of data acquisition to the conclusion of the steady-state regime. This test was carried out with an inlet airflow rate of 350 m $^3$ /h, a product airflow rate of 150 m $^3$ /h, an inlet DBT setpoint of 35 °C, and no humidification power applied.

It is observed that, prior to the operation of the AHU, the temperature and relative humidity sensors recorded values consistent with the ambient conditions of the laboratory (17 °C and 70–75 % RH in the example experimental test). Once the test started, these values evolved toward the new conditions, representative of the test setup, remaining practically constant over time. In the example case, the steady-state regime was maintained for approximately three hours; however, for all tests, only the average values obtained over a 20-minute period within the steady-state regime were used for the calculations. The secondary airflow in both measured zones was found to be saturated.

# 2.4. Performance parameters studied and uncertainties

The performance of the two-stage regenerative IEC prototype is studied in terms of the temperature drop, wet bulb and dew point thermal effectiveness, and cooling capacity.

The temperature drop is the dry bulb temperature difference between the air at the inlet  $T_{in}$  and the product air  $T_{ap}$ .

$$\Delta T = T_{in} - T_{qp} \tag{4}$$

The uncertainty of the temperature drop is estimated through the root sum squared (RSS) method [36], based on the uncertainty of the measuring equipment ( $u_T$ ), i.e. the accuracy of the calibrated sensor. After calibration, the uncertainty of the temperature sensors is improved from the accuracy given in Table 4 to  $u_T = 0.2\,^{\circ}\text{C}$ . Applying equation (5) yields an uncertainty in the temperature drop of 0.28 °C.

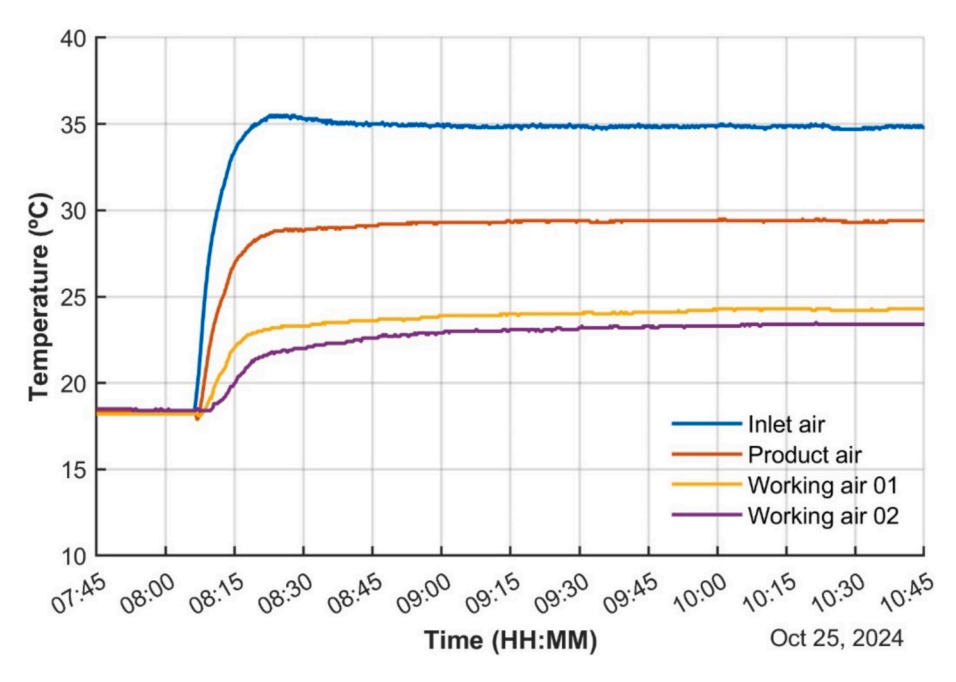


Fig. 4. Temperature evolutions on an example experimental test on October 25th, 2024.

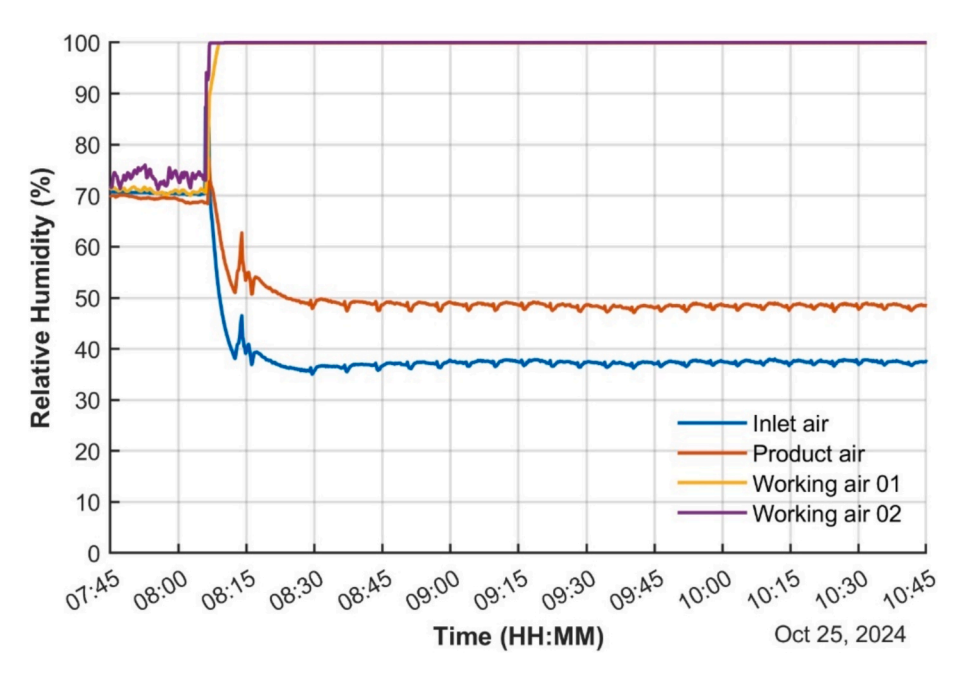


Fig. 5. Relative humidity evolutions on an example experimental test on October 25th, 2024.

$$u_{\Delta T} = \sqrt{\left(\frac{\partial \Delta T}{\partial T_{in}} u_T\right)^2 + \left(\frac{\partial \Delta T}{\partial T_{ap}} u_T\right)^2}$$
 (5)

The wet-bulb effectiveness relates the temperature drop (equation (4) to the wet bulb depression of the inlet air, as expressed by equation (6):

$$\varepsilon_{wb} = \frac{\Delta T}{T_{in} - T_{WBin}} \tag{6}$$

Given the iterative calculation of the wet-bulb temperature, the root sum squared method cannot be applied to the wet-bulb effectiveness. Alternatively, uncertainty was estimated as the maximum difference between the values obtained from the measurements and those achievable within the limits of accuracy of the measuring equipment ( $u_T = 0.2$  °C,  $u_{HR} = 0.2$  °C,  $u_{$ 

 $0.02\,\mathrm{per}-\mathrm{unit}$ ). The results show that the calculated values were always conservative and differed by less than  $0.09\,\mathrm{per}-\mathrm{unit}$ .

The dew-point depression relates the temperature drop achieved (equation (4) to the difference between the inlet air dry bulb ( $T_{in}$ ) and dew point ( $T_{DP\ in}$ ) temperatures:

$$\varepsilon_{dp} = \frac{\Delta T}{T_{in} - T_{DPin}} \tag{7}$$

According to the Root Sum Square (RSS) method, the uncertainty of the dew-point effectiveness is calculated by equation (8):

$$u_{\varepsilon_{DP}} = \sqrt{\left(\frac{\partial \varepsilon_{DP}}{\partial HR} u_{HR}\right)^2 + \left(\frac{\partial \varepsilon_{DP}}{\partial T_{in}} u_T\right)^2 + \left(\frac{\partial \varepsilon_{DP}}{\partial T_{qp}} u_T\right)^2}$$
(8)

A. Tejero-González et al. Energy & Buildings 348 (2025) 116431

Which, for the uncertainty of the instrumentation ( $u_T = 0.2^{\circ}\text{C}$ ,  $u_{HR} = 0.02$ ), is equal to 0.06 per unit.

Finally, the cooling capacity relates the temperature drop and the product air mass flow  $(\dot{m}_{ap})$  supplied by the system, hence provides useful insight on the actual cooling potential of the device:

$$CC = \dot{m}_{ap} \bullet (c_a + w_{in}c_v) \bullet \Delta T \tag{9}$$

where  $w_{in}$  is the inlet air humidity ratio, while  $c_a$  and  $c_v$  are the specific heat values of the dry air and vapor, respectively.

The uncertainty of the CC is calculated through equation (10):

$$u_{CC} = \sqrt{\left(\frac{\partial CC}{\partial \Delta p} u_{\Delta p}\right)^2 + \left(\frac{\partial CC}{\partial T_{in}} u_T\right)^2 + \left(\frac{\partial CC}{\partial T_{ap}} u_T\right)^2}$$
 (10)

Hence:

within  $\pm~2$  % of the humidity level (i.e. 29 %, 41 % or 59 %) shown in the graph. Results show that the temperature drop increase with higher DBT values and lower RH values at the inlet of the system. For instance, increasing the DBT from 25 °C to 40 °C at approximately constant 41 % relative humidity yields a temperature drop 1.8 times higher.

This behaviour is due to the larger evaporative cooling potential of drier and hotter air conditions. Although humidification is performed on the working airstream of the regenerative process (that is, at the psychrometric conditions of the treated air at the outlet, not at the inlet), the humidity ratio at both inlet and outlet of the treated air is the same, because the primary air undergoes a sensible process. Moreover, higher inlet air DBT will result in correspondingly higher DBT at the outlet. Combined with an identical humidity ratio, this leads to a larger wet bulb depression in the working air conditions at higher inlet DBT levels. The resulting Cooling Capacity (CC) follows the same trend as the temperature drop, ranging from an average of 138.6 W at 24.9 °C and 42 % RH to 324.4 W at 39.3 °C and 27 % RH.

$$u_{CC} = \mathscr{C} \bullet \sqrt{\left[\frac{1}{2 \bullet \sqrt{\Delta p}} \left(\frac{T_{in}}{T_{ap}} - 1\right) \bullet u_{\Delta p}\right]^2 + \left[\left(\frac{\sqrt{\Delta p}}{T_{ap}}\right) \bullet u_T\right]^2 + \left[\left(-\frac{\sqrt{\Delta p}}{T_{ap}^2}\right) \bullet u_T\right]^2}$$

$$(11)$$

Where:

$$\mathscr{C} = \frac{(c_a + w \cdot c_v) \bullet p_{atm} \bullet k}{R_a}$$
 (12)

Being  $p_{atm}$  the atmospheric pressure of the location (93200 Pa),  $R_a$  the gas constant for air (287.05  $J \cdot kg^{-1} \cdot K^{-1}$ ), and the specific heat of moist air is evaluated for the maximum humidity ratio (w) tested.

Equation (11) is applied for the maximum values of  $\Delta p$  and  $T_{\rm in}$ , but minimum  $T_{\rm ap}$ , because  $\frac{\partial CC}{\partial T_{\rm in}}$  and  $\frac{\partial CC}{\partial \Delta p}$  are increasing functions while  $\frac{\partial CC}{\partial T_{\rm op}}$  is a decreasing function. For the uncertainty introduced by the accuracy of the instrumentation ( $u_T=0.2^{\circ}{\rm C},\ u_{HR}=0.02,\ u_{\Delta p}=2\,{\rm Pa}$ ), the uncertainty of the cooling capacity is 24 W.

# 3. Results and discussion

# 3.1. Thermal performance of the two-stage prototype

Fig. 6 represents the temperature drop at different inlet DBT and RH. It should be noted that the actual measured RH in the represented tests is

The achieved temperature drop differences for varying inlet RH are smaller at lower inlet air DBT. In fact, while, at 30 °C, the difference in temperature drop between inlet RH of 59 % and 41 % is only 1 °C, at 35 °C, this difference increases up to 1.3 °C. Similarly, the difference between temperature drops at inlet RH of 41 % and 29 % is 1.3 °C at 35 °C, but reaches 1.9 °C at around 40 °C. This is due to the smaller differences in humidity ratios, and therefore in the enthalpies involved, when RH varies at lower DBT.

To better evaluate the effect of the inlet air relative humidity, tests were conducted at a wider range of RH while maintaining a constant inlet air, as shown in Fig. 7.a. The inlet air DBT was consistently measured at 34.6  $\pm$  0.2 °C, which corresponds to the measurement uncertainty  $u_T$ .

For a fixed inlet DBT, higher inlet air RH values also imply higher humidity ratios in the product air, thus in the working air driven to the wet channel. This hinders the evaporative cooling potential in the working air. Consequently, both the temperature drop achieved in the product air and the cooling capacity of the system decreases. The trend is almost linear, and a 20 % increase in the relative humidity results in a

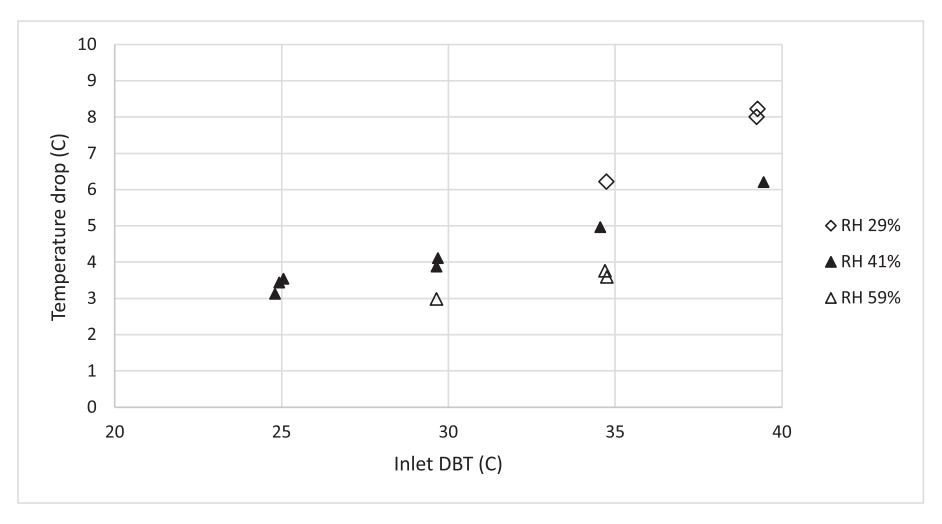


Fig. 6. Temperature drop achieved at different inlet DBT and RH (measured RH varying  $\pm$  2 %).

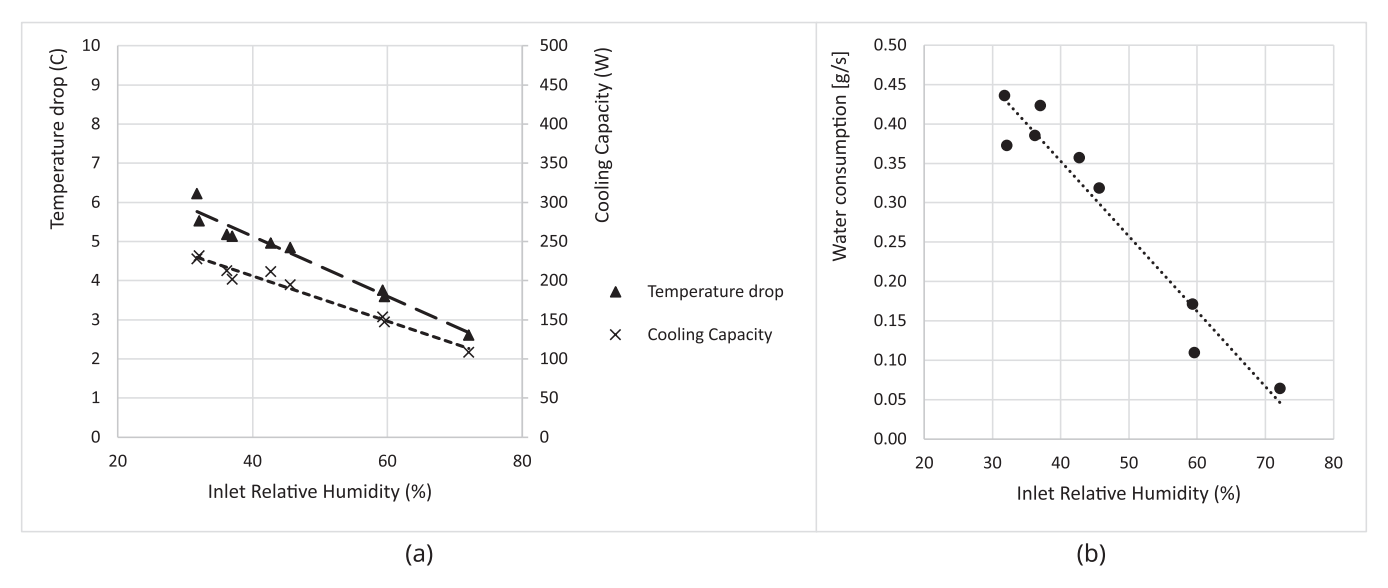


Fig. 7. (a) Temperature drop, Cooling capacity, and (b) water consumption variation with the inlet air RH at 34.6  $\pm$  0.2 °C inlet air DBT.

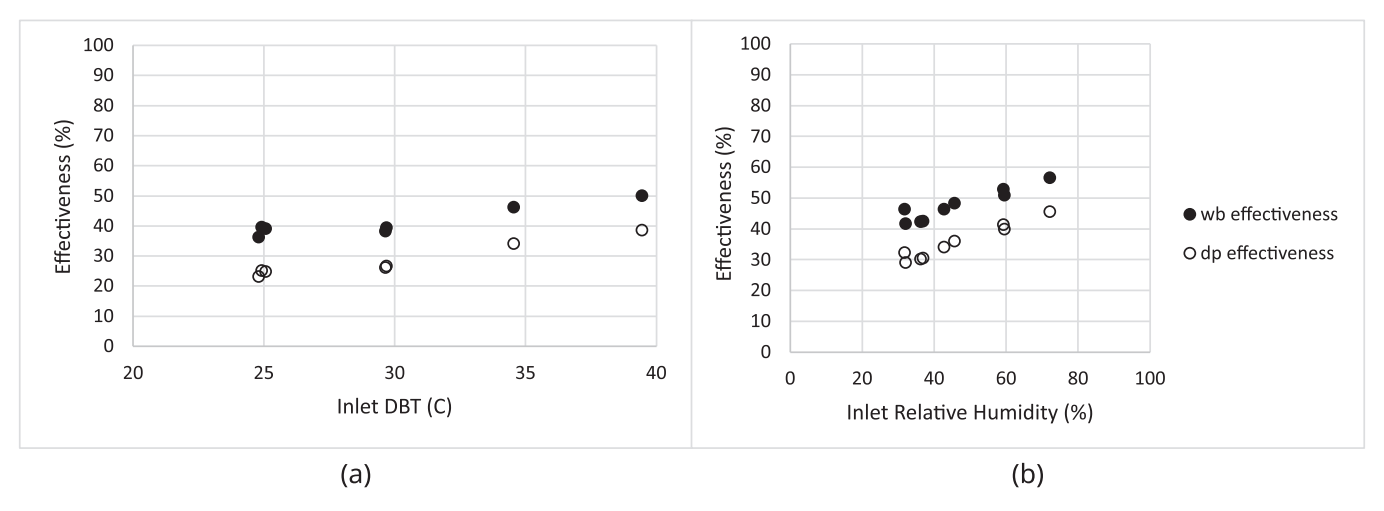


Fig. 8. A shows the influence of the inlet air dbt on the thermal effectiveness of the two-stage regenerative prototype at constant inlet air rh. the effect on both the wet bulb and the dew point effectiveness is smaller than what has been observed for the temperature drop in Fig. 6. On average, an increase in the DBT from 25 °C to 40 °C at approximately constant 41 % yields a wet bulb and dew point effectiveness 1.3 and 1.6 times higher, respectively. This result is due to the same definitions of both parameters (equations (6) and (7). The improvement in temperature drop achieved at larger inlet air DBT and constant RH is balanced by the larger wet bulb or dew point depression, respectively.

decrease of  $1.4\,^{\circ}\text{C}$  and  $58.2\,^{\circ}\text{W}$  in the temperature drop and the cooling capacity, respectively. This result confirms the limitation of a regenerative indirect evaporative cooling system in humid climates.

The water consumed by the system is instead represented in Fig. 7.b. The reduced evaporative cooling potential in the working air resulting from an increased RH at constant DBT is illustrated by the lower water evaporation. Beyond the values shown in this graph, the highest rate of water consumption was registered at 39.2  $^{\circ}\text{C}$  and 28 %, reaching 0.53 g/s, hence about 1.9 l/h.

Fig. 8.b illustrates that the effect of the inlet air RH at constant DBT is more noticeable. While Fig. 7 shows that a 20 % increase in the inlet air RH decreases the temperature drop by 30 %, Fig. 7.b indicates that the wet bulb and dew point effectiveness increase by 20 % and 30 %, respectively. This occurs because an increase in the inlet air RH significantly reduces the wet bulb and dew point depressions (affecting the denominator in equations 6 and 7)This effect prevails over the decrease caused in the temperature drop.

Fig. 8. Wet bulb and dry bulb thermal effectiveness of the two-stage regenerative IEC at (a) varied inlet DBT and constant  $41 \pm 2$  % inlet air

RH, and (b) varied inlet RH and approximately 35 °C inlet air DBT.

#### 3.2. Compared performance to previous one-stage prototype

Results of the performance of the present two-stage prototype are compared to a previously studied mixed-flow, one-stage device made of polycarbonate plates [27]. Dimensions of the polycarbonate heat exchanger of the one-stage prototype were 30 x 17 x 30 cm³, disregarding the outer insulation. In the cited work, different alternative constructions were studied, so in order to make a meaningful comparison, here it is taken as reference the device covered with cotton cloth on the wet side, tested with the same type of water distributor as the one used in the present work. Tests used in this comparison were conducted at an inlet air volume flow rate of 6.0  $\pm$  0.2 m³/min, which is comparable to that of the present study (5.9  $\pm$  0.2 m³/min).

Table 6 compares the performance for 30  $^{\circ}$ C and 35  $^{\circ}$ C inlet DBT at relative humidity of about 40 %. Figures provided for the two-stage prototype correspond to the average values obtained from the tests performed at these conditions. Results show that a two-stage device can

**Table 6**Thermal performance comparison between present two-stage and previous one-stage prototype, at 40% inlet air relative humidity.

Prototype	Temperature drop (ΔT) [°C]		Cooling Capacity (CC) [W]		Wet Bulb effectiveness ( $\varepsilon_{wb}$ ) [%]		Dew Point effectiveness ( $\varepsilon_{dp}$ ) [%]	
	DBT 30 °C	DBT 35 °C	DBT 30 °C	DBT 35 °C	DBT 30 °C	DBT 35 °C	DBT 30 °C	DBT 35 °C
Previous one-stage [27]	2.7	3.8	154.1	184.5	25.7	29.4	17.5	20.9
Present two-stage	4.0	5.0	169.7	211.9	39.8	46.4	27.0	34.2
Increment (%)	50 %	30 %	10 %	15 %	55 %	58 %	54 %	64 %

achieve larger temperature drops, hence better thermal effectiveness. The temperature drop increases by about 50 % at 30 °C inlet air DBT, while for the same RH at 35 °C that improvement reaches 30 %. This is due to the combined effect of the two-stages and the larger evaporative cooling potential in the humidified airstream. However, the improvement achieved in the Cooling Capacity is lower because of the larger rate of treated air that is diverted as working air in a two-stage design, which decreases the product air and thus jeopardises the cooling capacity despite achieving larger temperature drops. Indeed, the working-to-inlet air ratio for the two-stage design is around 0.6, while for the previous one-stage prototype it was 0.5. This result seems to agree with the literature [30], where it was stated that a multistage arrangement could enhance the thermal effectiveness at the expense of the cooling capacity.

Table 7 compares the effect of the inlet RH at a given inlet DBT on the performance of both prototypes. Values provided correspond to inlet air DBT of about 35  $^{\circ}$ C. The temperature drop and both types of effectiveness are about 1.5 times higher for the two-stage prototype operating at 32  $^{\circ}$ RH, and slightly better at higher RH of 45  $^{\circ}$ C. Once again, the improved performance of the two-stage prototype is much lower in terms of cooling capacity because of the larger design airflow that is diverted towards the wet channels working airflow.

A closer insight on the effect on the Cooling Capacity is shown in Table 8, where the values provided in previous Table 6 and Table 7 are provided in relation to the total heat exchange area of each prototype. The improvement in the cooling capacity of only 12–17 % shown in Table 7 does not compensate the 76 % larger heat exchange area of the device, resulting into 34–37 % lower CC/A. Because both prototypes operate with the same inlet air volume flows, the two-stage design, involving two bleed-off points, results into a higher working-to-inlet air ratio. This decreases the product air and hence the Cooling Capacity as defined in equation (9). Because, as seen in Table 6, increasing the inlet air DBT yielded slight improvements in the Cooling Capacity of the two-stage prototype, the decrease in its CC/A compared to the one-stage prototype is smaller at 35 °C than at 30 °C, even though the difference is minor and of limited practical significance. Equivalently, this smaller decrease in CC/A is observed at higher relative humidities of the inlet air

It is to be noted that the total useful volume of the heat exchanger in the one-stage device was 0.0153  $\,\mathrm{m}^3$ , while the two-stage device is larger, 0.0248  $\,\mathrm{m}^3$ . Regarding the cooling capacity relative to the useful volume of the device, at an inlet dry-bulb temperature of 35 °C and 32 % relative humidity, the two-stage prototype achieves 9.4 kW/m³, which is 31 % lower than that of the one-stage prototype. Under the same dry-bulb temperature but at 45 % relative humidity, the cooling capacity reaches only 7.9 kW/m³, representing a 28 % reduction compared to the one-stage prototype. Consequently, the studied two-stage device is preferred if higher temperature drops are sought, but the reference one-stage device would be preferable in terms of cooling capacity against the size of the equipment.

**Table 8**Cooling Capacity to heat exchange area. Comparison between present two-stage and previous one-stage prototype.

_								
Prototype	Heat exchange area	Cooling Capacity per heat exchange area (CC/A) $[W/m^2]$						
	A [m <sup>2</sup> ]	DBT 30 °C, RH 40 %	DBT 35 °C, RH 40 %	RH 32 %, DBT 35 °C	RH 45 %, DBT 35 °C			
Previous one- stage [27]	1.35	114.2	136.6	153.5	123.7			
Present two- stage	2.376	71.4	89.2	97.7	82.0			
Increment (%)	76 %	-37 %	-35%	-36%	-34 %			

# 3.3. Compared performance to experimental results in the literature

The literature on two-stage regenerative Indirect Evaporative Cooling (IEC) systems is limited and relies on simulations validated through experiments on one-stage devices. To the knowledge of the authors, the only exception is the work of Dizaji et al. [21] who experimentally validated a two-stage counter-flow regenerative IEC using a laboratory-scale test rig with a single pair of dry-wet channels.

Table 9 summarizes the main characteristics and operation results for the setup of Dizaji et al. and for the prototype studied in this work. Comparable inlet air DBT and humidity ratio conditions were selected from the available experimental tests.

By operating under a higher working-to-inlet air ratio (0.6) than the setup from Dizaji et al. [21], and with a significantly larger inlet airflow rate (10 times greater), the investigated prototype showed notable differences in performance: indeed, it achieved only two-thirds of the temperature drop reported by Dizaji et al. [21], but it also exhibited six times higher cooling capacity thanks to the higher inlet airflow.

These differences can be explained by having a closer look the dimensions and configuration of each device. The single pair dry-wet channels test rig (provided in ref. [21]) has a cross-sectional area of 8 cm² and a total heat exchange area of 0.2 m². In contrast, the present multi-channel prototype has cross-sectional area of 174.9 cm² and a total heat exchange area of 2.38 m². Thus, in both devices, the heat exchange area is between 22 and 24 m² per unit of inlet mass air flow rate; moreover, the normalized inlet air mass flow rate (i.e. the air mass flow rate per unit of cross-sectional area, representative of the mean air velocity in the dry channels) is here 5.6 kg/s per m², which is about half of the one used by Dizaji et al. (11.25 kg/s per m²). Furthermore, when normalized to the heat exchange area, the present specific cooling capacity (CC/A) is 137.9 W/m², which is again about half of that reported by Dizaji et al. (279 W/m²).

The lower temperature drops of the mixed-flow prototype, even

**Table 7** Thermal performance comparison between present two-stage and previous one-stage prototype, at constant 35 °C inlet DBT.

Prototype	Temperature drop (ΔT) [°C]		Cooling Capacity (CC) [W]		Wet Bulb effectiveness ( $\varepsilon_{wb}$ ) [%]		Dew Point effectiveness ( $\varepsilon_{dp}$ ) [%]	
	RH 32 %	RH 45 %	RH 32 %	RH 45 %	RH 32 %	RH 45 %	RH 32 %	RH 45 %
Previous one-stage [27]	3.8	3.2	207.3	167.0	28.1	31.0	19.8	23.2
Present two-stage	5.5	4.9	232.1	194.9	41.8	48.3	29.1	36.1
Increment (%)	48 %	51 %	12 %	17 %	49 %	56 %	47 %	55 %

**Table 9**Performance comparison between the present two-stage prototype and experimental results from literature [21].

Work	Configuration and materials	Inlet air DBT [°C]	Inlet humidity ratio (w <sub>in</sub> ) [g <sub>v</sub> /kg <sub>da</sub> ]	Inlet air mass flow rate [kg/s]	Working-to- inlet air ratio	Temp. drop ΔT [°C]	Cooling Capacity [W]
Dizaji et al. [21]	Two-stage regenerative, counter-flow. Nylon and tissue wicking.	40	9.65	0.009	0.5	12.0	55.8*
Present study	Two-stage regenerative, mixed flow. Polycarbonate and cotton wicking.	39.2	10.96	0.098	0.59	8.0	327.8

<sup>\*</sup>Cooling capacity is deduced from the data provided in the published work.

when operated at lower inlet air velocities and higher working air flow rates, suggest that there is room for design improvement. Mixed-flow configurations inherently have less efficient heat exchange compared to counter-flow designs, which benefit from more effective heat and mass transfer. However, counter-flow systems face practical challenges when scaled, due to the need for accommodation of multiple channels, three distinct air streams (with the corresponding inlet/outlet sections), and complex water distribution systems. The mixed-flow design, while less efficient, addresses these challenges and demonstrates feasibility for practical implementation.

Key factors influencing the performance are the working-to-inlet air ratio and the normalized airflow rate. In this study, a higher working-to-inlet air ratio reduced the product air flow, which in turn lowered the cooling capacity. Additionally, the present prototype operated with a lower normalized inlet airflow, contributing to a reduced specific cooling capacity (CC/A). However, the lower CC/A values observed in the tests do not necessarily indicate inferior cooling performance for the current prototype. If tested under comparable inlet air velocities and working-to-inlet air ratios, the results would likely be much closer to those of the reference system reported in [21].

Despite some limitations, this work advances the experimental validation of two-stage regenerative IECs, transitioning from single-channel laboratory setups to a multi-channel, technically and feasible prototype. The results highlight the potential for practical integration into larger HVAC systems, while identifying opportunities for further optimization in geometry, flow configuration, and operating parameters.

# 4. Conclusions

The present work proposes a new design of mixed-flow, two-stage regenerative Indirect Evaporative Cooler. This configuration contrasts with the cross-flow and counter-flow heat exchangers commonly investigated in the literature. Although cross flow cannot be designed into several stages, at least on a unique module, counter-flow designs can. However, only a few published works evaluated the effect of multiple stages, and most did so only through simulation models validated with experimental results on one-stage devices.

The regenerative configuration improves the thermal effectiveness beyond the wet bulb effectiveness. Designs with multiple stages can enhance this effect, ideally supplying the product air at the dew point temperature of the inlet airstreams. Indeed, the temperature drops achieved in the two-stage design here proposed are 30 % higher compared to a previously studied one-stage mixed-flow prototype, and the thermal effectiveness improves by up to 58 %.

However, because the main limitation of regenerative configurations is that they divert part of the treated air as working air, thus reducing the product airstream, the cooling capacity is a key factor to be evaluated. This effect is strengthened in multiple-stage designs. For instance, the two-stage prototype barely increases the cooling capacity to as much as 17 % compared to the previous one-stage design, due to the higher working-to-inlet air ratio (hence reduced product air flow rate). Moreover, the actual cooling capacity per heat exchange area is less advantageous in the case of the two-stage prototype. Consequently, a two-stage design will be preferable if higher temperature drops are sought,

but the improvement in the cooling capacity will not counterbalance the larger size.

The resulting present prototype is a  $0.025~\mathrm{m}^3$  device that supplies 40 l/s of product air. The experimental characterization for inlet air conditions between 25 °C and 40 °C dry bulb temperature and 30–70 % relative humidity, shows that increasing inlet DBT and decreasing inlet RH improve the temperature drop, cooling capacity, and thermal effectiveness, though with lower effect on the latter. These trends agree with the literature. Best performance of up to 8 °C temperature drops and over 320 W cooling rate is achieved for the harshest inlet air conditions of near 40 °C dry bulb temperature and 30 % relative humidity. Exploitation of this technology has significant potential in hot and dry climates, though auxiliary cooling may be needed to achieve thermal comfort. Additionally, water scarcity must be assessed, given the larger water consumptions of 1.9 l/h entrained when operating under these harsh inlet conditions.

Given the significant negative impact of increasing inlet air relative humidity on performance, the main limitation of this device, as with all indirect evaporative cooling systems operating in a regenerative configuration, is its applicability in humid climates. To address this limitation, integrating a desiccant process upstream of the device could be a viable solution. Alternatively, it may be worthwhile to compare the performance of the indirect evaporative cooler operating in the current regenerative configuration with that of a recuperative configuration using return air as the working airstream.

Compared to reference results from an alternative two-stage counterflow design studied at a laboratory test-rig, the achieved temperature drops are 33 % lower, while the cooling capacity per unit of heat exchange area is halved for the same inlet temperature and humidity conditions. However, differences in the inlet air velocities and the working-to-inlet air ratio within the compared tests point to promising performance results that should be confirmed in future research, suggesting a closer performance gap in terms of cooling capacity when upscaling two-stage devices from laboratory to practical conditioning units. Additionally, they reveal relevant room for design improvement to increase temperature drops. The current design results in a fixed minimum operating working-to-inlet air ratio. Since lower ratios may enhance the cooling capacity, it would be worthwhile to explore minor design modifications that allow reducing the achievable operating working-to-inlet air ratios. All in all, the proposed design presents the advantages of easy assembly and connection, as well as operation with larger airflow rates corresponding to practical applications.

# $CRediT\ authorship\ contribution\ statement$

Ana Tejero-González: Writing – original draft, Formal analysis, Data curation, Conceptualization. Manuel Andrés-Chicote: Writing – review & editing, Investigation, Formal analysis. Eloy Velasco-Gómez: Methodology, Investigation. Alessandra Urso: Investigation. Vincenzo Costanzo: Writing – review & editing, Formal analysis. Gianpiero Evola: Writing – review & editing, Formal analysis. Francesco Nocera: Writing – review & editing, Supervision.

#### Declaration of competing interest

The authors declare that they have no known competing financial interests or personal relationships that could have appeared to influence the work reported in this paper.

#### Acknowledgements

This work has been developed within the research project TED2021-129652A-C22, funded by MCIN/AEI/10.13039/501100011033 and the European Union through the "NextGenerationEU"/PRTR.

#### References

- A. Tejero-González, A. Franco-Salas, Direct evaporative cooling from wetted surfaces: Challenges for a clean air conditioning solution. Wiley Interdiscip Rev, Energy Environ. 11 (2022), https://doi.org/10.1002/wene.423.
- [2] ASHRAE. Chapter 41. Evaporative air-cooling equipment. ASHRAE Handbook. Systems and Equipment., 2020.
- [3] H. Yang, W. Shi, Y. Chen, Y. Min, Research development of indirect evaporative cooling technology: An updated review, Renew. Sustain. Energy Rev. 145 (2021), https://doi.org/10.1016/j.rser.2021.111082.
- [4] E. Velasco Gómez, A. Tejero González, F.J. Rey Martínez, Experimental characterisation of an indirect evaporative cooling prototype in two operating modes, Appl. Energy 97 (2012), https://doi.org/10.1016/j.apenergy.2011.12.065.
- [5] M.S. Alam, M.N. Mohd Zubir, M.MR. Bin, K.SN. Bin, H.F. Öztop, S. Abdullah, et al., A technological review of dew point evaporative cooling: experimental, analytical, numerical and optimization perspectives, Journal of Building Engineering 91 (2024), https://doi.org/10.1016/j.jobe.2024.109544.
- [6] X. Xiao, J. Liu, A state-of-art review of dew point evaporative cooling technology and integrated applications, Renew. Sustain. Energy Rev. 191 (2024), https://doi. org/10.1016/j.rser.2023.114142.
- [7] S. Kashyap, J. Sarkar, A. Kumar, Comparative performance analysis of different novel regenerative evaporative cooling device topologies, Appl. Therm. Eng. 176 (2020), https://doi.org/10.1016/j.applthermaleng.2020.115474.
- [8] H. Sadighi Dizaji, E.J. Hu, L. Chen, A comprehensive review of the Maisotsenkocycle based air conditioning systems, Energy 156 (2018) 725–749, https://doi.org/ 10.1016/j.energy.2018.05.086.
- [9] L. Lai, X. Wang, E. Hu, N.K. Choon, A vision of dew point evaporative cooling: Opportunities and challenges, Appl. Therm. Eng. 244 (2024), https://doi.org/ 10.1016/j.applthermaleng.2024.122683.
- [10] L. Jia, J. Liu, C. Wang, X. Cao, Z. Zhang, Study of the thermal performance of a novel dew point evaporative cooler, Appl. Therm. Eng. 160 (2019), https://doi. org/10.1016/j.applthermaleng.2019.114069.
- [11] C. Deepak, R. Naik, S.C. Godi, C.K. Mangrulkar, H.k. p., Thermal performance analysis of a mixed-flow indirect evaporative cooler, Appl. Therm. Eng. 217 (2022), https://doi.org/10.1016/j.applthermaleng.2022.119155.
- [12] M. Jradi, S. Riffat, Experimental and numerical investigation of a dew-point cooling system for thermal comfort in buildings, Appl. Energy 132 (2014) 524–535, https://doi.org/10.1016/j.apenergy.2014.07.040.
- [13] B. Riangvilaikul, S. Kumar, Numerical study of a novel dew point evaporative cooling system, Energy Build. 42 (2010) 2241–2250, https://doi.org/10.1016/j enbuild 2010 07 020
- [14] S.S. Baakeem, J. Orfi, A.A. Mohamad, Investigations of geometrical and operational aspects of a dew-point air-cooling system (M-cycle), Journal of Building Engineering 36 (2021), https://doi.org/10.1016/j.jobe.2020.102117
- [15] C. Zhan, Z. Duan, X. Zhao, S. Smith, H. Jin, S. Riffat, Comparative study of the performance of the M-cycle counter-flow and cross-flow heat exchangers for indirect evaporative cooling - Paving the path toward sustainable cooling of buildings, Energy 36 (2011) 6790–6805, https://doi.org/10.1016/j. energy.2011.10.019.
- [16] H. Jafarian, H. Sayyaadi, F. Torabi, Modeling and optimization of dew-point evaporative coolers based on a developed GMDH-type neural network, Energy Convers Manag 143 (2017) 49–65, https://doi.org/10.1016/j. enconman.2017.03.015.

- [17] M. Zhu, J. Lv, B. Zhou, W. Xi, L. Wang, E. Hu, Study on the performance of a novel dew-point evaporative cooler based on fiber membrane automatic wicking, Sci. Technol. Built Environ. 29 (2023) 574–587, https://doi.org/10.1080/ 23744731.2023.2194194.
- [18] F. Gao, K. Thu, S. Wang, F. Zhao, J. Lin, K. Wu, Numerical investigation of a novel tubular dew-point evaporative cooler, Appl. Therm. Eng. 223 (2023), https://doi. org/10.1016/j.applthermaleng.2023.120064.
- [19] A. Tejero-González, M. Andrés-Chicote, E. Velasco-Gómez, F.J. Rey-Martínez, Influence of constructive parameters on the performance of two indirect evaporative cooler prototypes, Appl. Therm. Eng. 51 (2013), https://doi.org/ 10.1016/j.applthermaleng.2012.10.054.
- [20] H. Sadighi Dizaji, E.J. Hu, L. Chen, S. Pourhedayat, Development and validation of an analytical model for perforated (multi-stage) regenerative M-cycle air cooler, Appl. Energy 228 (2018) 2176–2194, https://doi.org/10.1016/j. appergy 2018 07 018
- [21] H. Sadighi Dizaji, E.J. Hu, L. Chen, S. Pourhedayat, Analytical/experimental sensitivity study of key design and operational parameters of perforated Maisotsenko cooler based on novel wet-surface theory, Appl. Energy 262 (2020), https://doi.org/10.1016/j.apenergy.2020.114557.
- [22] Y. Wan, T. Xue, Z. Huang, A. Soh, H. Liu, K.J. Chua, Comparative study on performance of counter-flow dew-point indirect evaporative cooling systems via a more realistic and experimentally validated three-dimensional model, Journal of Building Engineering 82 (2024), https://doi.org/10.1016/j.jobe.2023.108408.
- [23] W. Shi, H. Yang, X. Ma, X. Liu, A novel indirect evaporative cooler with porous media under dual spraying modes: A comparative analysis from energy, exergy, and environmental perspectives, Journal of Building Engineering 76 (2023), https://doi.org/10.1016/j.jobe.2023.106874.
- [24] T. Sun, X. Huang, Y. Chen, H. Zhang, Experimental investigation of water spraying in an indirect evaporative cooler from nozzle type and spray strategy perspectives, Energy Build. 214 (2020), https://doi.org/10.1016/j.enbuild.2020.109871.
- [25] X. Ma, W. Shi, H. Yang, Spray parameter analysis and performance optimization of indirect evaporative cooler considering surface wettability, Journal of Building Engineering 82 (2024), https://doi.org/10.1016/j.jobe.2023.108175.
- [26] P. Xu, X. Ma, X. Zhao, K. Fancey, Experimental investigation of a super performance dew point air cooler, Appl. Energy 203 (2017) 761–777, https://doi. org/10.1016/j.apenergy.2017.06.095.
- [27] A. Urso, E. Velasco-Gómez, A. Tejero-González, M. Andrés-Chicote, F. Nocera, Experimental study of the optimal design and performance of a mixed-flow dewpoint indirect evaporative cooler, Appl. Therm. Eng. 257 (2024), https://doi.org/ 10.1016/j.applthermaleng.2024.124294.
- [28] B. Zhou, J. Lv, M. Zhu, L. Wang, L. Liang, Q. Chen, Simulation study of a thin membrane inclined automatic wicking dew-point evaporative cooling device, Journal of Building Engineering 72 (2023), https://doi.org/10.1016/j. jobe.2023.106601.
- [29] B. Zhou, J. Lv, M. Zhu, L. Wang, S. Li, E. Hu, Experiment for the performance of a thin membrane inclined automatic wicking dew-point evaporative cooling device based on simulation results, Energy Build. 308 (2024), https://doi.org/10.1016/j. enbuild 2024 114021
- [30] X. Cui, X. Yang, Q. Kong, X. Meng, L. Jin, Performance evaluation and comparison of multistage indirect evaporative cooling systems in two operation modes, Int. J. Energy Res. 44 (2020) 9298–9308, https://doi.org/10.1002/er.4803.
- [31] X. Cui, M.R. Islam, B. Mohan, K.J. Chua, Developing a performance correlation for counter-flow regenerative indirect evaporative heat exchangers with experimental validation, Appl. Therm. Eng. 108 (2016) 774–784, https://doi.org/10.1016/j. applthermaleng.2016.07.189.
- [32] S.J. Oh, M.W. Shahzad, M. Burhan, W. Chun, C. Kian Jon, M. KumJa, et al., Approaches to energy efficiency in air conditioning: A comparative study on purge configurations for indirect evaporative cooling, Energy 168 (2019) 505–515, https://doi.org/10.1016/j.energy.2018.11.077.
- [33] X. Liu, C. Jing, Y. Zhao, T. Miyazaki, Numerical study on performance of the dew point evaporative cooling system, J. Therm. Sci. Technol. 16 (2021), https://doi. org/10.1299/jtst.2021jtst0040.
- [34] S. Anisimov, D. Pandelidis, J. Danielewicz, Numerical analysis of selected evaporative exchangers with the Maisotsenko cycle, Energy Convers Manag 88 (2014) 426–441, https://doi.org/10.1016/j.enconman.2014.08.055.
- [35] D.H.W. Li, W. Pan, J.C. Lam, A comparison of global bioclimates in the 20th and 21st centuries and building energy consumption implications, Build. Environ. 75 (2014) 236–249, https://doi.org/10.1016/j.buildenv.2014.02.009.
- [36] R.J. Moffat, Describing the Uncertainties in Experimental Results, Standford University, Stanford, California, 1988.